Solid State Communications 371 (2023) 115265

Contents lists available at ScienceDirect

Solid State Communications

journal homepage: www.elsevier.com/locate/ssc

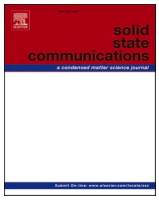

Landau level transition and magnetophonon resonance in a twisted bilayer graphene

Matthew DeCapua [a], Yueh-Chun Wu [a], Takashi Taniguchi [b], Kenji Watanabe [c], Jun Yan [a,*]

[a] Department of Physics, University of Massachusetts Amherst, Amherst, MA, 01003, USA
[b] Research Center for Materials Nanoarchitectonics, National Institute for Materials Science, 1-1 Namiki, Tsukuba, 305-0044, Japan
[c] Research Center for Electronic and Optical Materials, National Institute for Materials Science, 1-1 Namiki, Tsukuba, 305-0044, Japan

ARTICLE INFO

Communicated by: Francois Peeters

Keywords:
A:Twisted graphene
D:Landau levels
D:magnetophonon
E:Raman spectroscopy

ABSTRACT

We perform resonant Raman spectroscopy on 8° twisted bilayer graphene placed in an out-of-plane magnetic field. The high-quality device has narrow Landau level linewidth of less than 5 meV that enables detection of features from both electronic Raman scattering and magnetophonon resonance involving electronic transitions between the low energy Landau levels. Two magnetophonon resonances are observed, one at 4.6T in the strong coupling regime, and the other at 2.6T in the weak coupling regime. Using the measured Landau level transition energy, we analyze the renormalization of effective band velocity, whose dependence on magnetic field points to a 20% enhancement of dielectric constant due to the presence of an adjacent graphene layer, a quite prominent screening effect from a monolayer of carbon atoms in proximity. Both the Landau level transition electronic Raman and the magnetophonon resonance are gate tunable. Harnessing angular momentum conservation, we demonstrate charge tuning of electron phonon coupling strength for left and right circularly polarized G band phonons separately.

1. Introduction

Since the realization of superconductivity [1] and correlated insulating states [2] in magic-angle twisted bilayer graphene, there has been a renewed effort to understand the role of electron-phonon coupling and many-body interactions in these systems [3–9]. Raman scattering is an experimental tool particularly well suited for such an investigation because it allows for the direct observation of phonon modes and can be used in conjunction with electric and magnetic fields for highly tunable experiments [10–16]. When a two-dimensional material such as graphene is subjected to an out-of-plane magnetic field, its electronic states quench into discrete energy plateaus known as Landau levels, which have prominent effects on both electronic and optical properties of the system [17–23]. These Landau levels also participate in light scattering processes, both directly as intrinsic excitations or via coupling with a phonon in a Raman scattering event [10,12–15,20,24–28]. Experimentally accessible Landau level spectroscopy is a useful tool for understanding many-body interactions in the system, such as renormalization of the effective band velocity in the presence of an external magnetic field [11,25].

Although Raman scattering is typically weak for atomically thin materials such as graphene, twisted graphene is known to possess van Hove singularities which produce exciton states [29–32] that can result in more than an order of magnitude increase in the intensity of Raman scattering at resonance [33–37]. When a relative twist angle between the two graphene layers is introduced, the Dirac cones corresponding to the different layers become offset in momentum-space. The van Hove singularities arise from an avoided crossing where these cones overlap, and thus the exciton energy is sensitive to twist angle [29]. We can exploit this enhancement of the scattering cross section to improve the signal-to-noise ratio by carefully selecting the excitation wavelength to resonate with these excitons.

In this work, using a twisted graphene with van Hove singularities producing an optical resonance at around 1.59 eV, we investigate Landau level transitions and magnetophonon resonances in the system via resonant Raman scattering. We observe the emergence of a peak that blueshifts as the square root of the applied field which we ascribe to electronic scattering between Landau levels 1 and -1, labeled as $LL_{-1,1}$. We also see a modulation of the graphene G Raman mode (~1590 cm^{-1}) at 2.6 T and 4.6 T, consistent with magnetophonon resonance between the phonon and $LL_{-2,3}$ (or $LL_{-3,2}$ by particle-hole symmetry) and $LL_{-1,2}$ ($LL_{-2,1}$) respectively. The prominent effects of the three Landau level

* Corresponding author.
E-mail address: yan@physics.umass.edu (J. Yan).

https://doi.org/10.1016/j.ssc.2023.115265
Received 30 April 2023; Received in revised form 19 June 2023; Accepted 22 June 2023
Available online 27 June 2023

transitions reflect the high quality of our twisted graphene device, evidenced by the narrow Landau level linewidth that is less than 5 meV. Competition between the imaginary part of the Landau level self-energy and electron-phonon coupling strength dictates that the magnetophonon resonance at 4.6 T is in the strong coupling regime where mode anti-crossing is observed, while the one at 2.6 T is in the weak regime where the magnetophonon exhibits a crossover from blueshift to redshift. Both the $LL_{-1,1}$ electronic Raman mode and the magnetophonon resonance can be tuned by a gate voltage. In particular, we demonstrate that we can tune the electron-phonon coupling strength of left-handed G band phonon markedly without changing that for the right-handed G phonon, and vice versa, essentially lifting the two-fold degeneracy of the G band phonon. These measurements reflect the opposite angular momentum of the $LL_{-1,2}$ and $LL_{-2,1}$ transitions, as well as the requirement of angular momentum conservation in the electron-phonon coupling process.

2. Device characterization

Fig. 1a shows an optical microscope image of our device. The twisted graphene sample was fabricated by the standard "tear-and-stack" technique [38] and sandwiched between hexagonal boron nitride (hBN) sitting on top of a 30 nm WSe_2 back gate. The top hBN (15 nm thickness) and bottom hBN (60 nm) and WSe_2 were carefully selected to provide a clean optical background and to enhance optical signal by constructive thin-film interference. The twist angle between the graphene layers is about 8°. At this angle, the incoming resonance with the "bright" exciton is accessible by Ti:Sapphire tunable laser. Fig. 1b shows the evolution of the G-band (1590 cm^{-1} at 4 K; all spectra presented herein were taken at 4 K inside a liquid helium cryostat) spectra as the wavelength is tuned into resonance around 768 nm, showing a strong enhancement of intensity relative to that of the hBN Raman peak, while the latter decreases with increasing wavelength according to the $\sim 1/\lambda^4$ scattering law. Additionally, at the resonant excitation of 768 nm, we observe two weak phonon modes nearby the G band main peak, corresponding to the superlattice activated R_{TO} and R_{LO} Raman modes at 1554 cm^{-1} and 1630 cm^{-1} respectively. The presence of the LO phonon at the moiré wavevector at a higher energy than the zero momentum G mode reflects the Kohn anomaly effect in the graphene electron-phonon coupled system [39–41].

Applying an out-of-plane magnetic field to our twisted bilayer graphene, we generate Landau level transitions and magnetophonon resonances with clear experimental signatures in the Raman spectrum. Fig. 1c shows circular polarization resolved Raman spectra of our device in a magnetic field of 6 T. The in-plane lattice vibration of hBN and graphene G band has a quasi-angular momentum of magnitude $\hbar$, and they appear in the cross-circular polarization channel [40,42]. The weak G band in co-circular spectrum is due to finite extinction ratio of ~40:1 for our optical system. It is also interesting to note that R_{TO} and R_{LO} do not have good circular selection rule, consistent with their finite moiré momentum nature. In the co-circular scattering channel, an additional Raman mode appears at 1470 cm^{-1} (182 meV) with a 19 ± 2 cm^{-1} (2.4 ± 0.3 meV) HWHM (half width at half maximum) activated by the magnetic field. Its absence in the cross-circular polarization channel indicates that it has 0 angular momentum. Transitions between Landau levels LL_n and LL_m involve a transfer net 0 angular momentum for $|n| = |m|$, while transitions with $|n| - |m| = \pm 1$ involve a non-zero transfer of angular momentum [13]. We thus attribute the new mode to the $LL_{-1,1}$ transition.

3. Results and discussion

3.1. Magnetic field dependence of the Landau level transition

Fig. 2a shows magnetic field dependence of unpolarized Raman spectra between 4.5 and 9 T where we observe two prominent magnetic field dependent features in the Raman spectrum of our twisted bilayer graphene sample. The first is the emergence of $LL_{-1,1}$. The second is a modification of the G phonon lineshape, attributed to coupling between the phonon and a magnetoexciton. We first address the $LL_{-1,1}$ electronic transition. Since the van Hove singularity arising from the layer twist is at a much higher energy than the Landau level in question, we assume at low energy the two graphene layers are approximately decoupled, and fit the energy evolution to the Landau level spectrum of monolayer graphene $E_n = v_F\sqrt{2|n|\hbar eB}$ in a single particle picture, where e is the elementary unit of charge, and B is the strength of the applied field. For transitions between levels −1 and 1, the energy is thus

$$E_{-1,1} = 2v_F\sqrt{2\hbar eB} \quad (1)$$

Fitting Fig. 2b with Eq. (1) gives a reasonably good description of the data and yields a Fermi velocity of $v_F = 1.02 \times 10^6 m/s$, consistent with previous studies of monolayer graphene [26,43].

On the other hand, the slight underestimation of the fit at low fields and overestimation at high fields suggests a magnetic field dependent band velocity that can be accounted for by many-body interactions. (Another possible interpretation is the opening of a band gap due to possible inversion symmetry breaking in our device; see supplementary.) Theoretical studies reveal that electron-electron interactions renormalize the band dispersion and result in the band velocity being replaced by an effective velocity that varies with the applied field [25,44,45]. The first order correction to the velocity is given by a perturbative expansion around the effective fine-structure constant $\alpha_\varepsilon \equiv (c/v_0)(\alpha/\varepsilon)$: $v = v_0\left(1 - \frac{\alpha_\varepsilon}{4}\ln\frac{|E|}{W}\right) = v_0 - \frac{\alpha c}{4\varepsilon}\ln\frac{|E|}{W}$, where v_0 is the bare velocity, $\alpha \approx 1/137$ is the fine structure constant, E is the electron energy, W is the

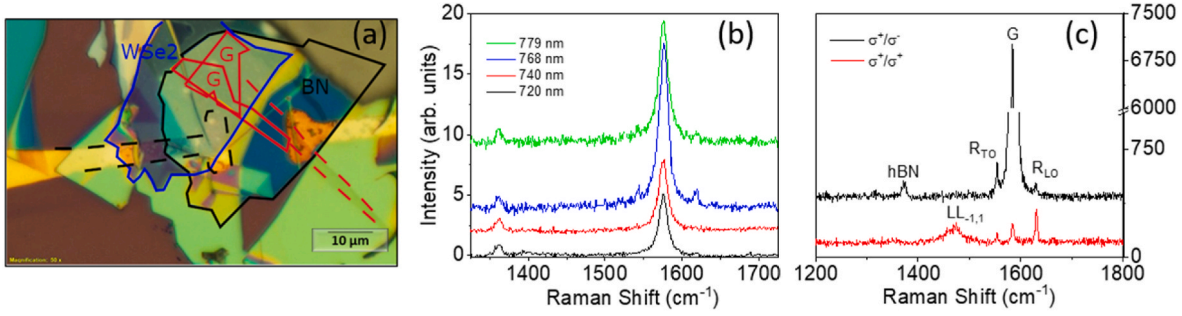

Fig. 1. Characterizing the twisted bilayer graphene sample
(a) An optical micrograph of the sample. (b) The evolution of the G band with laser excitation wavelength. The resonance with the moiré exciton at 768 nm is evident from the increased G band intensity relative to the hBN peak. The spectra are normalized so that the hBN peak has unit intensity. (c) Raman spectra showing the selection rules for cross- (black) and cocircular (red) polarization for both the phonon Raman modes (hBN, R_{TO}, R_{LO}, and G) and the electronic Landau level transition ($LL_{-1,1}$) at 6 T. (For interpretation of the references to color in this figure legend, the reader is referred to the Web version of this article.)

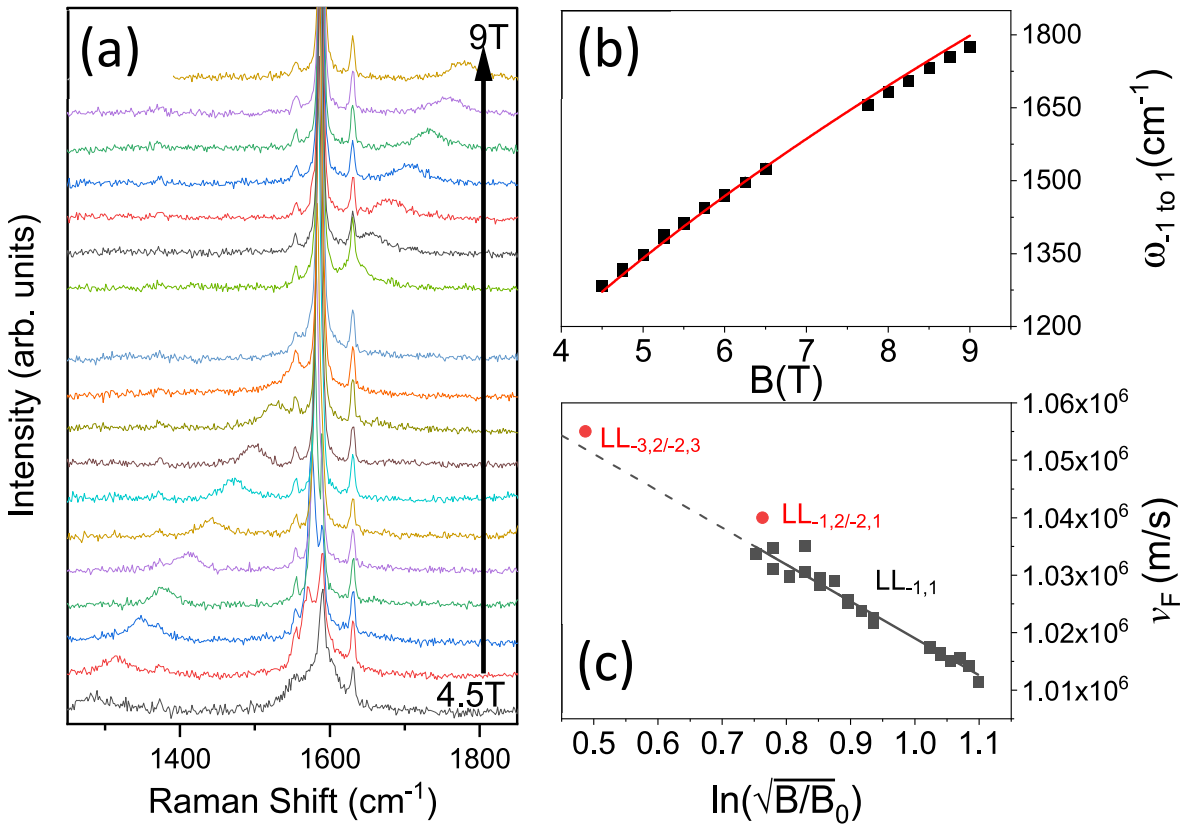

Fig. 2. Magnetic Field Dependence
(a) Unpolarized Raman spectra taken in a range of magnetic fields from 4.5 T to 9 T in 0.25 T increments. (b) The energy of the Landau level transition as a function of field. It is fit (red line) by $2v_F\sqrt{2\hbar eB}$, with the fermi velocity $v_F = 1.02 \times 10^6$ m/s as the fit parameter. (c) Evolution of the fermi velocity with field for −1 to 1 Landau level transition (black squares). B_0 is taken to be 1 T. The fit (black line) reasonably agrees with the fermi velocities determined from the magnetophonon resonances (red circles) at 2.6 T and 4.6 T. (For interpretation of the references to color in this figure legend, the reader is referred to the Web version of this article.)

high-energy cutoff, and ε is the effective dielectric constant of the surrounding medium [25]. The factor of 4 comes from the degeneracy of the Landau level. The velocity of the interband transition $LL_{-n,n}$, is thus $v_n \sim \ln\frac{l_{B_0}}{l_B} = \ln\sqrt{\frac{B}{B_0}}$, where B_0 is an arbitrary reference field which we set to 1 T, with the constant of proportionality equal to $-\frac{\alpha c}{4\varepsilon}$:

$$\frac{dv_F}{dln\sqrt{\frac{B}{B_0}}} = -\frac{\alpha c}{4\varepsilon} \tag{2}$$

The dependence of band velocity renormalization on the dielectric constant ε reflects the sensitivity of electron-electron interactions to screening. Previous studies indeed find that the band velocity can be modulated by changing the dielectric environment of graphene [25]. In Fig. 2c we plotted the extracted v_F versus $\ln\sqrt{\frac{B}{B_0}}$. From the linear fit to Eq. (2) we find a slope of $(6.4 \pm 0.3)\times10^6$ m/s. This enabled us to extract an effective dielectric constant of $\varepsilon = 8.5 \pm 0.4$. It is instructive to compare this with values for monolayer graphene encapsulated in hBN (7.0 ± 0.5) and monolayer graphene on graphite (12 ± 1) [25]. That we see a larger ε than monolayer encapsulated by hBN is consistent with the increase in screening from the additional conducting graphene layer in our experiment. Quantitatively this 20% enhancement of dielectric constant is a quite remarkable effect from just one single sheet of atoms, due to proximity of the screening layer.

3.2. Magneto-phonon resonances

We also observe a dramatic change in the lineshape of the G phonon due to resonance with the magnetoexciton. Selection rules dictate that the phonon can couple to magnetoexcitons originating from $LL_{n,m}$ transitions, where $|n|-|m| = \pm1$. This coupling results in the emergence of two magnetophonon branches flanking the G phonon in the Raman spectrum. In monolayer graphene near the resonance, the magneto-phonon energy is well approximated by a coupled-mode model [10,27].

$$E_{\pm} = \frac{E_{me} + E_{ph}}{2} \pm \sqrt{\left(\frac{E_{me} - E_{ph}}{2}\right)^2 + g^2} \tag{3}$$

where $E_{\pm}$ are the energies of the two magnetophonon branches, $E_{me} = \Omega + i\Gamma$ is the complex energy of the magnetoexciton including the broadening Γ, E_{ph} is the complex energy of the bare phonon, and g is the electron-phonon coupling constant. We can express g in terms of the dimensionless coupling constant λ: $g = \sqrt{\frac{\lambda}{2}}E_1 = v_F\sqrt{e\hbar B\lambda}$.

Fig. 3 shows magneto-phonon resonance Raman spectra evolution for fields around 4.75 T, where we decompose the magnetophonon resonance into the bare G phonon and the two coupled modes. (Note that the bare G phonon has an intrinsic asymmetry, due to interference between the phonon and the spectrum of electronic excitations [46]. In practice we fit the shape by two Lorentzians, centered at 1583.7 cm^{-1} and 1588.3 cm^{-1} respectively.) The extracted MPR coupled mode energy and halfwidth are plotted in Fig. 3b and c respectively. This resonance corresponds to the interaction of the G band with the $LL_{-1,2}$ and $LL_{-2,1}$ transitions.

We simultaneously fit the position and linewidth of the magneto-phonon peaks using Eq. (3). E_{ph} is fixed to $197 + i0.6$ meV, with the real and imaginary parts experimentally determined from the centroid and half-width, respectively, of the G band at 0T. The free parameters are thus the band velocity, which determines the real part energy of the

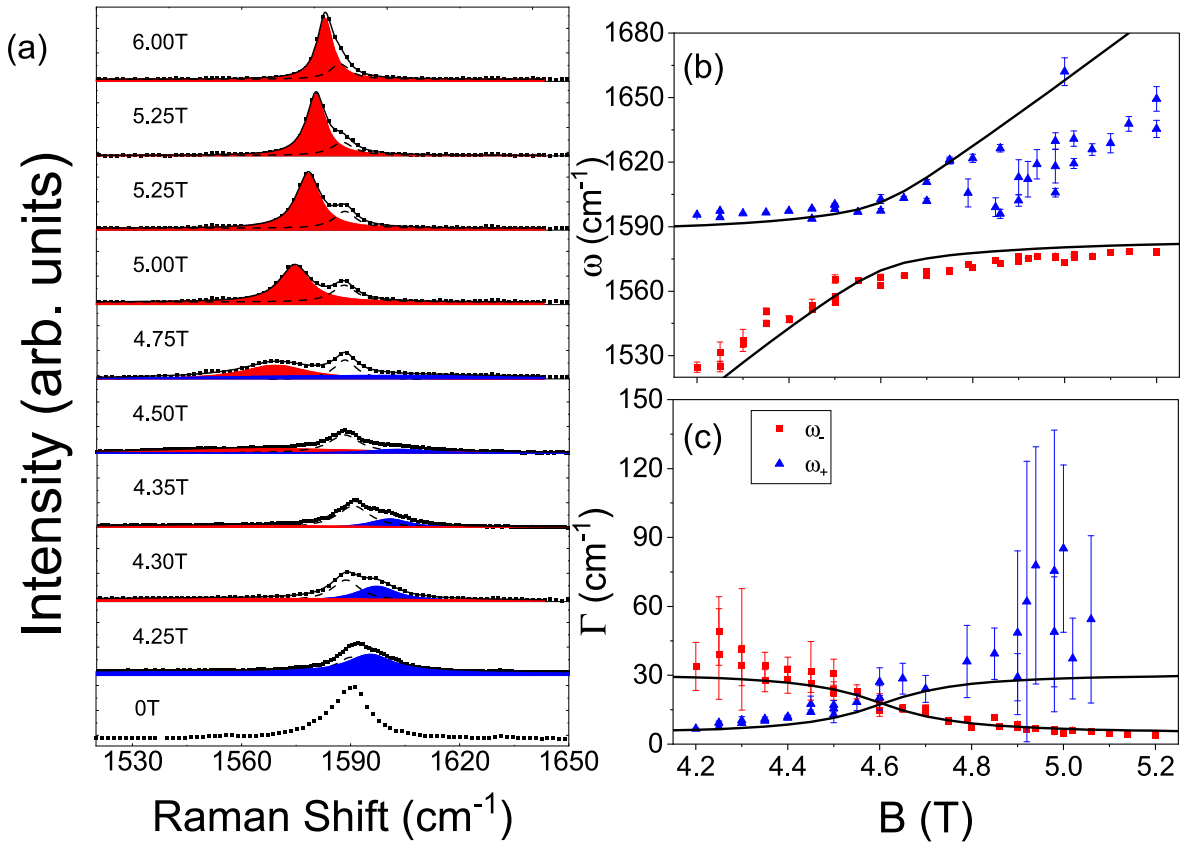

Fig. 3. $LL_{-1,2}$ ($LL_{-2,1}$) Magnetophonon Resonance (MPR) (a) Selected cross-circular polarization Raman spectra showing the evolution of the MPR with $LL_{-1,2}$ ($LL_{-2,1}$) with field. The red (lower energy) and blue (higher energy) curves highlight the two branches of the coupled-mode model (see text). The dashed line shows the intrinsic 0T component of the G phonon which is subtracted when fitting the magnetophonons to Lorentzians. (b) Peak position and (c) linewidth as a function of field for the two magnetophonon branches are fit (black lines) simultaneously to the coupled-mode model. (For interpretation of the references to color in this figure legend, the reader is referred to the Web version of this article.)

magnetoexciton; the imaginary part of the magnetoexcition energy, which sets the linewidth; and the electron-phonon coupling constant. The best fit of the coupled mode model is achieved for $v_F = 1.04 \times 10^6$ m/s, $\Gamma = 3.8 \pm 1.6$ meV, and coupling constant $\lambda = (1.8 \pm 0.2) \times 10^{-3}$. At resonance, we then extrapolate $\hbar\omega_+ = 198.9 + i4.4$ meV and $\hbar\omega_- = 195 + i4.4$ meV. We note that the coupling constant falls below previously reported values for single-layer graphene on SiO_2 ($(4.5 \pm 0.5) \times 10^{-3}$) [28] and graphene on graphite (6.36×10^{-3}) [10], in contrast to the strong electron-phonon coupling in magic-angle bilayer graphene [7,8].

Using the band velocity obtained from evolution of the $LL_{-1,1}$ in Fig. 2b, the resonance with the $LL_{-1,2}$ ($LL_{-2,1}$) transition is expected at 4.8 T. However, our MPR fit shows the resonance at 4.6 T, corresponding to a band velocity of 1.04×10^6 m/s, about 2% higher than the band velocity derived from the $LL_{-1,1}$ evolution. This result is consistent with experiments by Faugeras et al. where they observed higher band velocity for higher energy transitions, which was explained in terms of vertex corrections [25]. We have placed this Fermi velocity value as a red dot in Fig. 2c. Interestingly, this point falls reasonably well with the line fit of Fermi velocities extracted from the $LL_{-1,1}$ transitions.

For fields between near 2.6 T, we observed another MPR due to resonance with the $LL_{-3,2}$ and $LL_{-2,3}$ transitions, as shown in data in Fig. 4a. The modulation to spectral lineshape in this case is less dramatic than MPR in Fig. 3. This is because the resonance occurs at a lower magnetic field, and the coupling parameter g is smaller, due to the smaller Landau level degeneracy. The smaller g pushes this resonance into the weak coupling regime where the term in the square root in Eq. (3) becomes negative at resonance. Thus, unlike the repelling behavior in Fig. 3b, the MPR spectrum here is dominated by the mode with smaller linewidth, and we fit our data as a sum of the bare G phonon and a single Lorentzian peak, as shown in Fig. 4. The energy of the peak plotted in Fig. 4b crosses over from blue shift to red shift as the field increases, similar to a previous study [14].

By fitting the peak energy and linewidth using Eq. (2), we find the imaginary part of the $LL_{-3,2}$ ($LL_{-2,3}$) magnetoexciton self-energy, 4.05 ± 0.45 meV, and the electron-phonon coupling constant, $(1.5 \pm 0.2) \times 10^{-3}$. The coupling constant agrees within error with the values determined by the $LL_{-1,2}$ ($LL_{-2,1}$) fit. We note that the imaginary part of magnetoexciton self-energy we extracted for all three Landau level transitions $LL_{-1,1}$, $LL_{-1,2}$, and $LL_{-2,3}$ is consistently less than 5 meV, much narrower than graphene on SiO_2, and comparable to graphene on graphite, suspended graphene, and graphene sandwiched between hBN [19–21,24,25], confirming the high quality of our twisted graphene device. The resonance magnetic field occurs at 2.6T, corresponding to a band velocity of 1.06×10^6 m/s. This is 4% larger than the value extracted from Fig. 2b, and a further enhancement from the value extracted from $LL_{-1,2}$. As shown in Fig. 2c, the two independent measurements of MPR and $LL_{-1,1}$ transitions give consistent magnetic field dependence of the Fermi velocity, as set by the dielectric environment of the graphene device (solid and dashed lines in Fig. 2c).

3.3. *Gate tuning of Landau level transition and magneto-phonon resonance*

Both the $LL_{-1,1}$ Raman mode and the MPR involve electronic transition from a valence band LL to a conduction band LL, whose charge carrier population can be modulated by applying an external gate voltage. Fig. 5a shows the evolution of the $LL_{-1,1}$ peak with gate. Beyond

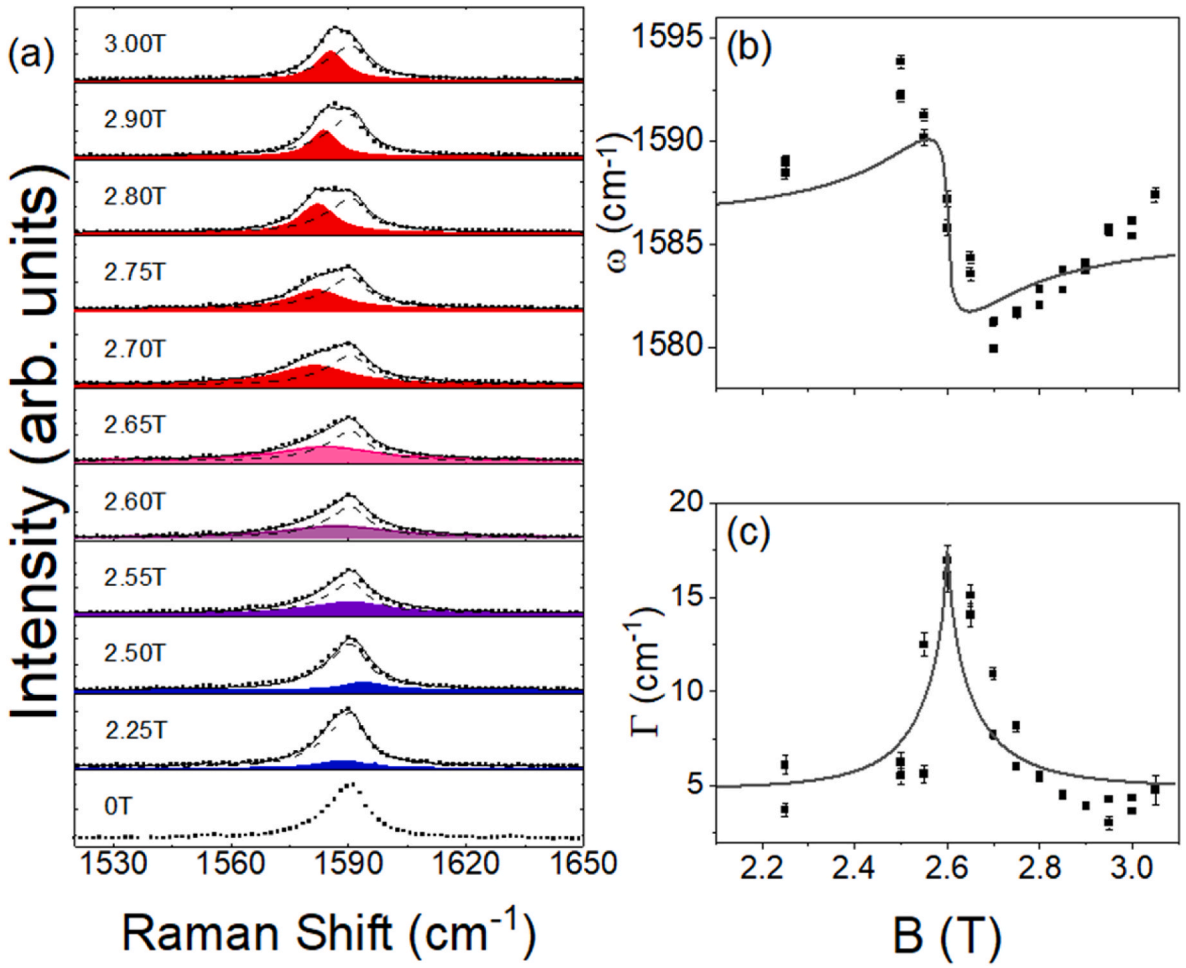

Fig. 4. $LL_{-2,3}$ ($LL_{-3,2}$) Magnetophonon Resonance (MPR) (a) Selected spectra demonstrating the evolution of the $LL_{-2,3}$ ($LL_{-3,2}$) with field. The reduced degeneracy due to smaller field results in weak coupling and the appearance of a single magnetophonon branch. The (b) position and (c) linewidth as a function of field are plotted for this branch and fit simultaneously to the coupled-mode model.

a certain voltage, the peak becomes quenched. This is the voltage at which LL_1 (LL_{-1}) begins to be populated with electrons (holes), which Pauli blocks the transition and causes it to become less intense, as the density of available states to support the transition is reduced [47]. In contrast, tuning the carrier concentration at lower density range amounts to modulating population of the 0^{th} LL (Fig. 5b left subpanel), which does not impact the $LL_{-1,1}$ transition. In Fig. 5c we normalize the intensity of $LL_{-1,1}$ to R_{LO}, which shows roughly constant Raman intensity over this gate tuning range. By performing a piecewise linear fit of the intensity profile as a function of gate (Fig. 5c), we can extrapolate the onset of the first Landau level at several B fields to determine the doping response to an applied electric field (data for other fields in Supplementary). We find the onset voltage for LL_1 and LL_{-1}, corresponding to filling factor $\nu = 2$ and -2 respectively, are to good approximation symmetric about 0V, indicating that our sample is intrinsically close to charge neutral. The filling factor is determined by the carrier density σ and the magnetic field B and is given by $\nu = 2\pi l_B^2 \sigma$. From the fit, $|\nu| = 2 = 0.35[T^{-1}]B$, we can extract $\sigma = 1.38 \times 10^{11}\ (V \bullet cm^2)^{-1}$ for V in volts. This is in reasonable agreement with our initial estimation of $\sigma(V) = 1.74 \times 10^{11}(V \bullet cm^2)^{-1}$ obtained by modeling our sample as a simple capacitor, with the hBN layer separating the graphene from the WSe_2 back gate acting as the dielectric.

While the $LL_{-1,1}$ transition is symmetric with respect to positive and negative charge doping, $LL_{-2,1}$ and $LL_{-1,2}$ are not. When the Fermi energy is set between LL_1 and LL_2 (Fig. 5b middle panel), versus between LL_{-1} and LL_{-2} (Fig. 5b right panel), the $LL_{-1,2}$ transition is allowed in the former case and forbidden in the latter. Noting that $LL_{-1,2}$ and $LL_{-2,1}$ transitions carry opposite angular momentum of $\pm\hbar$ due to the valley-antisymmetric nature of the magnetoexciton, by selectively exciting phonons of left- or right-handed helicity with circularly polarized light we can control which transition participates in the Raman scattering. Fig. 5d shows spectra using σ^- excitation with σ^+ collection (σ^-/σ^+) that measures left circularly polarized G band phonon which couples to $LL_{-1,2}$, but not $LL_{-2,1}$, as determined by angular momentum conservation. The three spectra at gate voltages of 4, 0 and −4 V, corresponding roughly to filling factors around 4, 0 and −4, are shown in Fig. 5d. The asymmetry between 4V and -4V is self-evident. In particular, the energy separation between the lower energy MPR mode and the bare G phonon is larger at -4V and smaller at 4V. Similarly, probing right-handed phonons with σ^+/σ^- reveals a larger separation for 4V and a smaller separation for -4V (see supplementary).

In Fig. 5e, we plot this gate dependent energy separation as a proxy for the electron-phonon coupling (see Eq [3]) for both σ^-/σ^+ (black squares) and σ^+/σ^- (red dots) channels. As the gate is tuned between filling factor −2 and filling factor 2, i.e., the 0^{th} Landau level, the coupling is roughly constant. Once the filling factor is tuned above 2, the coupling for the σ^-/σ^+ channel (black squares) becomes suppressed as less $LL_{-2,1}$ transition is available, while σ^+/σ^- channel (red dots) coupling remains high. Conversely, in the σ^+/σ^- channel (red dots), the electron-phonon coupling starts to decrease appreciably from filling factor −2, when LL_{-1} begins to be populated with holes and the $LL_{-1,2}$ transition is suppressed, and in this case the σ-/σ+ channel (black

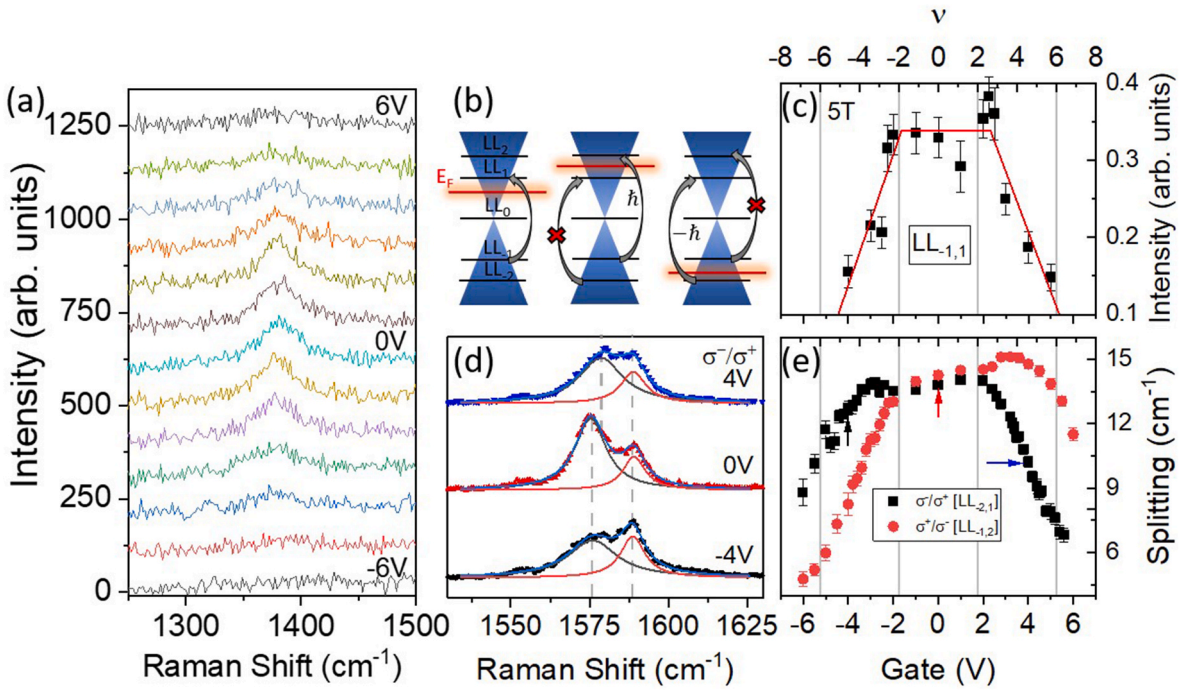

Fig. 5. Gate Dependence and Pauli Blocking Landau Level transitions
(a) The electronic Raman scattering from the $LL_{-1,1}$ transition taken at different gate voltages from -6V to 6V. When the gate is tuned so that the occupation of LL_{-1} or LL_1 is changing, the transition becomes suppressed and the Raman signature quenches. (b) Schematic illustration of allowed and forbidden $LL_{-1,1}$, $LL_{-1,2}$ and $LL_{-2,1}$ transitions. $LL_{-1,1}$ has 0 angular momentum while the other two have finite angular momentum. (c) Intensity evolution as a function of gate for data in (a). The red lines are fits. The grey lines roughly demarcate filling factors 2 and -2. (d) Asymmetric magnetophonon coupling with gate. The dashed lines are to aid in comparing relative positions of the magnetophonon peak. (e) The energy separation between the G phonon and the magnetophonon as a function of the gate. The arrows are color coordinated to the spectra in panel (d). All data were taken at 5 T. (For interpretation of the references to color in this figure legend, the reader is referred to the Web version of this article.)

squares) coupling remains high. Qualitatively, the data agree with the above description that circularly polarized G band phonon coupling with magnetoexciton is modulated only when the population of corresponding −1 or 1 Landau level participating in the transition is tuned by the gate voltage. However, there appears to be some anomalous response of $LL_{-1,2}$ ($LL_{-2,1}$) when the occupation of LL_1 (LL_{-1}) is tuned. We would expect the gate response in this regime to resemble tuning within LL_0, where the coupling is mostly unchanged by varying occupation of LLs which are not involved in the transition. Instead, the peak separation is seen to increase until LL_1 (LL_{-1}) reaches around half-filled ($\nu \approx \pm 4$), at which point the separation decreases. It is possible that sample inhomogeneity, including its asymmetric gating structure, might result in asymmetric doping of the two graphene layers. This could have ramifications for the overall electronic structure resulting in the observed deviations in coupling.

4. Conclusions

We employed resonant Raman scattering to investigate Landau level transitions and magnetophonon resonance in an 8° twisted bilayer graphene. Analysis of the Landau level transition energies and associated Fermi velocities reveal a prominent screening effect due to proximity to another graphene layer. Magnetophonon resonance of both strong coupling and weak coupling are observed that reveal consistent, albeit weaker, coupling strength than previous studies in related systems. The electron phonon coupling strength in the magnetophonon resonance is gate tunable. Our circular polarization resolved measurements reveal that the two-fold degeneracy of left- and right-handed G band under magnetophonon resonance is lifted when charge density in −1 or 1 Landau level is modulated. This demonstrates that $LL_{-1,2}$ and $LL_{-2,1}$ have nonzero and opposite angular momentum, and that their interaction with phonons respect angular momentum conservation.

Credit author statement

Matthew DeCapua: Conceptualization, Methodology, Data curation, Investigation, Formal analysis, Writing – original draft. Yueh-Chun Wu: sample preparation, Methodology, Software. Takashi Taniguchi: hBN crystal preparation. Kenji Watanabe: hBN crystal preparation. Jun Yan: Supervision, Writing- Reviewing and Editing.

Declaration of competing interest

The authors declare that they have no known competing financial interests or personal relationships that could have appeared to influence the work reported in this paper.

Data availability

Data will be made available on request.

Acknowledgement

This work is supported by the National Science Foundation (DMR-2004474). K.W. and T.T. acknowledge support from the JSPS KAKENHI (Grant Numbers 20H00354, 21H05233 and 23H02052) and World Premier International Research Center Initiative (WPI), MEXT, Japan.

Appendix A. Supplementary data

Supplementary data to this article can be found online at https://doi.org/10.1016/j.ssc.2023.115265.

References

[1] Y. Cao, V. Fatemi, S. Fang, K. Watanabe, T. Taniguchi, E. Kaxiras, P. Jarillo-Herrero, Unconventional superconductivity in magic-angle graphene superlattices, Nature 556 (2018) 43–50, https://doi.org/10.1038/nature26160.

[2] Y. Cao, V. Fatemi, A. Demir, S. Fang, S.L. Tomarken, J.Y. Luo, J.D. Sanchez-Yamagishi, K. Watanabe, T. Taniguchi, E. Kaxiras, R.C. Ashoori, P. Jarillo-Herrero, Correlated insulator behaviour at half-filling in magic-angle graphene superlattices, Nature 556 (2018) 80–84, https://doi.org/10.1038/nature26154.

[3] H. Polshyn, M. Yankowitz, S. Chen, Y. Zhang, K. Watanabe, T. Taniguchi, C. R. Dean, A.F. Young, Large linear-in-temperature resistivity in twisted bilayer graphene, Nat. Phys. 15 (2019) 1011–1016, https://doi.org/10.1038/s41567-019-0596-3.

[4] Y.W. Choi, H.J. Choi, Dichotomy of electron-phonon coupling in graphene moiré flat bands, Phys. Rev. Lett. 127 (2021), 167001, https://doi.org/10.1103/PhysRevLett.127.167001.

[5] A.C. Gadelha, D.A.A. Ohlberg, C. Rabelo, E.G.S. Neto, T.L. Vasconcelos, J. L. Campos, J.S. Lemos, V. Ornelas, D. Miranda, R. Nadas, F.C. Santana, K. Watanabe, T. Taniguchi, B. van Troeye, M. Lamparski, V. Meunier, V.H. Nguyen, D. Paszko, J.C. Charlier, L.C. Campos, L.G. Cançado, G. Medeiros-Ribeiro, A. Jorio, Localization of lattice dynamics in low-angle twisted bilayer graphene, Nature 590 (2021) 405–409, https://doi.org/10.1038/s41586-021-03252-5.

[6] G.S.N. Eliel, M.V.O. Moutinho, A.C. Gadelha, A. Righi, L.C. Campos, H.B. Ribeiro, P.W. Chiu, K. Watanabe, T. Taniguchi, P. Puech, M. Paillet, T. Michel, P. Venezuela, M.A. Pimenta, Intralayer and interlayer electron-phonon interactions in twisted graphene heterostructures, Nat. Commun. 9 (2018) 1221, https://doi.org/10.1038/s41467-018-03479-3.

[7] A.C. Gadelha, V.H. Nguyen, E.G.S. Neto, F. Santana, M.B. Raschke, M. Lamparski, V. Meunier, J.C. Charlier, A. Jorio, Electron-phonon coupling in a magic-angle twisted-bilayer graphene device from gate-dependent Raman spectroscopy and atomistic modeling, Nano Lett. 22 (2022) 6069–6074, https://doi.org/10.1021/acs.nanolett.2c00905.

[8] Y.W. Choi, H.J. Choi, Strong electron-phonon coupling, electron-hole asymmetry, and nonadiabaticity in magic-angle twisted bilayer graphene, Phys. Rev. B 98 (2018), 241412, https://doi.org/10.1103/PhysRevB.98.241412.

[9] F. Wu, A.H. Macdonald, I. Martin, Theory of phonon-mediated superconductivity in twisted bilayer graphene, Phys. Rev. Lett. 121 (2018), 257001, https://doi.org/10.1103/PhysRevLett.121.257001.

[10] J. Yan, S. Goler, T.D. Rhone, M. Han, R. He, P. Kim, V. Pellegrini, A. Pinczuk, Observation of magnetophonon resonance of Dirac fermions in graphite, Phys. Rev. Lett. 105 (2010), 227401, https://doi.org/10.1103/PhysRevLett.105.227401.

[11] J. Sonntag, S. Reichardt, L. Wirtz, B. Beschoten, M.I. Katsnelson, F. Libisch, C. Stampfer, Impact of many-body effects on landau levels in graphene, Phys. Rev. Lett. 120 (2018), 187701, https://doi.org/10.1103/PhysRevLett.120.187701.

[12] Y. Kim, J.M. Poumirol, A. Lombardo, N.G. Kalugin, T. Georgiou, Y.J. Kim, K. S. Novoselov, A.C. Ferrari, J. Kono, O. Kashuba, V.I. Fal'Ko, D. Smirnov, Measurement of filling-factor-dependent magnetophonon resonances in graphene using Raman spectroscopy, Phys. Rev. Lett. 110 (2013), 227402, https://doi.org/10.1103/PhysRevLett.110.227402.

[13] O. Kashuba, V.I. Fal'Ko, Signature of electronic excitations in the Raman spectrum of graphene, Phys. Rev. B Condens. Matter 80 (2009), 241404, https://doi.org/10.1103/PhysRevB.80.241404.

[14] C. Faugeras, M. Amado, P. Kossacki, M. Orlita, M. Sprinkle, C. Berger, W.A. De Heer, M. Potemski, Tuning the electron-phonon coupling in multilayer graphene with magnetic fields, Phys. Rev. Lett. 103 (2009), 186803, https://doi.org/10.1103/PhysRevLett.103.186803.

[15] Y. Kim, Y. Ma, A. Imambekov, N.G. Kalugin, A. Lombardo, A.C. Ferrari, J. Kono, D. Smirnov, Magnetophonon resonance in graphite: high-field Raman measurements and electron-phonon coupling contributions, Phys. Rev. B Condens. Matter 85 (2012), 121403, https://doi.org/10.1103/PhysRevB.85.121403.

[16] S. Goler, J. Yan, V. Pellegrini, A. Pinczuk, Raman spectroscopy of magneto-phonon resonances in graphene and graphite, Solid State Commun. 152 (2012) 1289–1293, https://doi.org/10.1016/j.ssc.2012.04.020.

[17] K.S. Novoselov, A.K. Geim, S.V. Morozov, D. Jiang, M.I. Katsnelson, I. V. Grigorieva, S.V. Dubonos, A.A. Firsov, Two-dimensional gas of massless Dirac fermions in graphene, Nature 438 (2005) 197–200, https://doi.org/10.1038/nature04233.

[18] Y. Zhang, Y.W. Tan, H.L. Stormer, P. Kim, Experimental observation of the quantum Hall effect and Berry's phase in graphene, Nature 438 (2005) 201–204, https://doi.org/10.1038/nature04235.

[19] M. Orlita, C. Faugeras, P. Plochocka, P. Neugebauer, G. Martinez, D.K. Maude, A. L. Barra, M. Sprinkle, C. Berger, W.A. De Heer, M. Potemski, Approaching the Dirac point in high-mobility multilayer epitaxial graphene, Phys. Rev. Lett. 101 (2008), 267601, https://doi.org/10.1103/PhysRevLett.101.267601.

[20] Z. Jiang, E.A. Henriksen, L.C. Tung, Y.J. Wang, M.E. Schwartz, M.Y. Han, P. Kim, H.L. Stormer, Infrared spectroscopy of landau levels of graphene, Phys. Rev. Lett. 98 (2007), 197403, https://doi.org/10.1103/PhysRevLett.98.197403.

[21] B.J. Russell, B. Zhou, T. Taniguchi, K. Watanabe, E.A. Henriksen, Many-particle effects in the cyclotron resonance of encapsulated monolayer graphene, Phys. Rev. Lett. 120 (2018), 047401, https://doi.org/10.1103/PhysRevLett.120.047401.

[22] L. Ju, L. Wang, X. Li, S. Moon, M. Ozerov, Z. Lu, T. Taniguchi, K. Watanabe, E. Mueller, F. Zhang, D. Smirnov, F. Rana, P.L. McEuen, Unconventional valley-dependent optical selection rules and landau level mixing in bilayer graphene, Nat. Commun. 11 (2020) 2941, https://doi.org/10.1038/s41467-020-16844-y.

[23] J. Pack, B.J. Russell, Y. Kapoor, J. Balgley, J. Ahlers, T. Taniguchi, K. Watanabe, E. A. Henriksen, Broken symmetries and kohn's theorem in graphene cyclotron resonance, Phys. Rev. X 10 (2020), 41006, https://doi.org/10.1103/PhysRevX.10.041006.

[24] C. Faugeras, M. Amado, P. Kossacki, M. Orlita, M. Kühne, A.A.L. Nicolet, Y. I. Latyshev, M. Potemski, Magneto-Raman scattering of graphene on graphite: electronic and phonon excitations, Phys. Rev. Lett. 107 (2011), 036807, https://doi.org/10.1103/PhysRevLett.107.036807.

[25] C. Faugeras, S. Berciaud, P. Leszczynski, Y. Henni, K. Nogajewski, M. Orlita, T. Taniguchi, K. Watanabe, C. Forsythe, P. Kim, R. Jalil, A.K. Geim, D.M. Basko, M. Potemski, Landau level spectroscopy of electron-electron interactions in graphene, Phys. Rev. Lett. 114 (2015), 126804, https://doi.org/10.1103/PhysRevLett.114.126804.

[26] C. Neumann, S. Reichardt, M. Drögeler, B. Terrés, K. Watanabe, T. Taniguchi, B. Beschoten, S.V. Rotkin, C. Stampfer, Low B field magneto-phonon resonances in single-layer and bilayer graphene, Nano Lett. 15 (2015) 1547–1552, https://doi.org/10.1021/nl5038825.

[27] M.O. Goerbig, J.N. Fuchs, K. Kechedzhi, V.I. Fal'Ko, Filling-factor-dependent magnetophonon resonance in graphene, Phys. Rev. Lett. 99 (2007), 087402, https://doi.org/10.1103/PhysRevLett.99.087402.

[28] S. Rémi, B.B. Goldberg, A.K. Swan, Charge tuning of nonresonant magnetoexciton phonon interactions in graphene, Phys. Rev. Lett. 112 (2014), 056803, https://doi.org/10.1103/PhysRevLett.112.056803.

[29] R.W. Havener, Y. Liang, L. Brown, L. Yang, J. Park, Van hove singularities and excitonic effects in the optical conductivity of twisted bilayer graphene, Nano Lett. 14 (2014) 3353–3357, https://doi.org/10.1021/nl500823k.

[30] W. Yan, M. Liu, R.F. Dou, L. Meng, L. Feng, Z.D. Chu, Y. Zhang, Z. Liu, J.C. Nie, L. He, Angle-dependent van Hove singularities in a slightly twisted graphene bilayer, Phys. Rev. Lett. 109 (2012), 126801, https://doi.org/10.1103/PhysRevLett.109.126801.

[31] G. Li, A. Luican, J.M.B. Lopes Dos Santos, A.H. Castro Neto, A. Reina, J. Kong, E. Y. Andrei, Observation of Van Hove singularities in twisted graphene layers, Nat. Phys. 6 (2010) 109–113, https://doi.org/10.1038/nphys1463.

[32] H. Patel, L. Huang, C.J. Kim, J. Park, M.W. Graham, Stacking angle-tunable photoluminescence from interlayer exciton states in twisted bilayer graphene, Nat. Commun. 10 (2019) 1445, https://doi.org/10.1038/s41467-019-09097-x.

[33] K. Kim, S. Coh, L.Z. Tan, W. Regan, J.M. Yuk, E. Chatterjee, M.F. Crommie, M. L. Cohen, S.G. Louie, A. Zettl, Raman spectroscopy study of rotated double-layer graphene: misorientation-angle dependence of electronic structure, Phys. Rev. Lett. 108 (2012), 246103, https://doi.org/10.1103/PhysRevLett.108.246103.

[34] M.C. DeCapua, Y.C. Wu, T. Taniguchi, K. Watanabe, J. Yan, Probing the bright exciton state in twisted bilayer graphene via resonant Raman scattering, Appl. Phys. Lett. 119 (2021), https://doi.org/10.1063/5.0049458.

[35] R. He, T.F. Chung, C. Delaney, C. Keiser, L.A. Jauregui, P.M. Shand, C.C. Chancey, Y. Wang, J. Bao, Y.P. Chen, Observation of low energy Raman modes in twisted bilayer graphene, Nano Lett. 13 (2013) 3594–3601, https://doi.org/10.1021/nl4013387.

[36] J. Bin Wu, X. Zhang, M. Ijäs, W.P. Han, X.F. Qiao, X.L. Li, D.S. Jiang, A.C. Ferrari, P.H. Tan, Resonant Raman spectroscopy of twisted multilayer graphene, Nat. Commun. 5 (2014) 5309, https://doi.org/10.1038/ncomms6309.

[37] W.X. Luo, X.L. Liu, X. Chen, H. Wu, X. Cong, M.L. Lin, P.H. Tan, A tunable Raman system based on ultrafast laser for Raman excitation profile measurement, Rev. Sci. Instrum. 92 (2021) 3–6, https://doi.org/10.1063/5.0059099.

[38] K. Kim, M. Yankowitz, B. Fallahazad, S. Kang, H.C.P. Movva, S. Huang, S. Larentis, C.M. Corbet, T. Taniguchi, K. Watanabe, S.K. Banerjee, B.J. Leroy, E. Tutuc, Van der Waals heterostructures with high accuracy rotational alignment, Nano Lett. 16 (2016) 1989–1995, https://doi.org/10.1021/acs.nanolett.5b05263.

[39] S. Piscanec, M. Lazzeri, F. Mauri, A.C. Ferrari, J. Robertson, Kohn anomalies and electron-phonon interactions in graphite, Phys. Rev. Lett. 93 (2004), 185503, https://doi.org/10.1103/PhysRevLett.93.185503.

[40] J. Maultzsch, S. Reich, C. Thomsen, H. Requardt, P. Ordejón, Phonon dispersion in graphite, Phys. Rev. Lett. 92 (2004), 075501, https://doi.org/10.1103/PhysRevLett.92.075501.

[41] S.Y. Zhou, D.A. Siegel, A.V. Fedorov, A. Lanzara, Kohn anomaly and interplay of electron-electron and electron-phonon interactions in epitaxial graphene, Phys. Rev. B Condens. Matter 78 (2008), 193404, https://doi.org/10.1103/PhysRevB.78.193404.

[42] S. Reich, A.C. Ferrari, R. Arenal, A. Loiseau, I. Bello, J. Robertson, Resonant Raman scattering in cubic and hexagonal boron nitride, Phys. Rev. B Condens. Matter 71 (2005), 205201, https://doi.org/10.1103/PhysRevB.71.205201.

[43] A. Luican, G. Li, A. Reina, J. Kong, R.R. Nair, K.S. Novoselov, A.K. Geim, E. Y. Andrei, Single-layer behavior and its breakdown in twisted graphene layers, Phys. Rev. Lett. 106 (2011), 126802, https://doi.org/10.1103/PhysRevLett.106.126802.

[44] K. Shizuya, Many-body corrections to cyclotron resonance in monolayer and bilayer graphene, Phys. Rev. B Condens. Matter 81 (2010), 075407, https://doi.org/10.1103/PhysRevB.81.075407.

[45] D.C. Elias, R.V. Gorbachev, A.S. Mayorov, S.V. Morozov, A.A. Zhukov, P. Blake, L. A. Ponomarenko, I.V. Grigorieva, K.S. Novoselov, F. Guinea, A.K. Geim, Dirac cones reshaped by interaction effects in suspended graphene, Nat. Phys. 7 (2011) 701–704, https://doi.org/10.1038/nphys2049.

[46] E.H. Hasdeo, A.R.T. Nugraha, M.S. Dresselhaus, R. Saito, Breit-Wigner-Fano line shapes in Raman spectra of graphene, Phys. Rev. B Condens. Matter 90 (2014), 245140, https://doi.org/10.1103/PhysRevB.90.245140.

[47] P. Kossacki, C. Faugeras, M. Kühne, M. Orlita, A. Mahmood, E. Dujardin, R.R. Nair, A.K. Geim, M. Potemski, Circular dichroism of magnetophonon resonance in doped graphene, Phys. Rev. B Condens. Matter 86 (2012), 205431, https://doi.org/10.1103/PhysRevB.86.205431.